

Time delays between the soft and hard X-ray bands in GRS 1915+105

A. Janiuk¹*, B. Czerny¹

¹*Nicolaus Copernicus Astronomical Centre, Bartycka 18, 00-716 Warsaw, Poland*

19 June 2018

ABSTRACT

The hard X-ray lightcurves exhibit delays of ~ 1 s with respect to the soft X-ray lightcurves when the microquasar GRS 1915+105 is in the state of frequent, regular outbursts (states ρ and κ of Belloni et al. 2000). Such outbursts are supposed to be driven by the radiation pressure instability of the inner disc parts. The hard X-ray delays are then caused by the time needed for the adjustment of the corona to changing conditions in the underlying disc. We support this claim by the computation of the time evolution of the disc, including a non-stationary evaporation of the disc and mass exchange with the corona.

Key words: accretion, accretion discs – black hole physics, instabilities, stars – binaries – close, X-rays

1 INTRODUCTION

The observations of Galactic black hole binaries (GBH) imply the coexistence of a relatively cold, optically thick accretion disc, responsible for a thermal disc-blackbody component in their soft X-ray spectra, with a hot, optically thin medium that is the source of power-law spectral tail in the hard X-ray band (see e.g. Done 2002 for a review). At least in the High and Very High spectral states, the latter may have the form of a corona above the accretion disc, which means that the geometrical configuration of these two media is such that both are extending down to the last stable orbit around the black hole, being vertically separated from each other. The hard X-rays are produced via Compton upscattering of seed photons coming from the underlying disc, which basically requires the energy dissipation within the corona. Apart from this radiative coupling, also a mass transfer, i.e. evaporation and condensation of matter between the disc and corona is possible (Meyer & Meyer-Hofmeister 1994; Rózańska & Czerny 2000).

Radiation pressure instability (e.g. Taam & Lin 1984; Lasota & Pelat 1991) seems to be a plausible mechanism to account for the characteristic variability of the Galactic microquasar GRS 1915+105 (Mirabel & Rodriguez 1994; Taam, Chen & Swank 1997; Belloni et al. 2000). Exemplary lightcurves were analyzed recently by Naik et al. (2002). Some of these lightcurves exhibit a very regular shape of outbursts, that can be possibly related to the disc variability, while others are more chaotic and probably driven by other mechanism, e.g. jet emission. Time-dependent accre-

tion disc model with jet emission was studied e.g. by Nayakshin et al. (2000) and Janiuk et al. (2002). Recently, Watarai & Mineshige (2003) analyzed the oscillations of this source allowing for the temporary evacuation of the inner disc.

If the disc instability is the primary cause of regular outbursts, we may expect that the hard X-ray coronal emission would be significantly delayed with respect to the soft X-ray disc emission. In the present paper we check the hypothesis of the radiation pressure instability as the outburst driver by analyzing the observed time delays between the soft and hard X-ray emission. We study the behaviour of GRS 1915+105 in various variability classes. We compare the observed time delays with the exemplary results of our theoretical model. In this model we compute numerically the time evolution of the disc-corona system with the mass exchange between the two media.

The structure of this article is as follows. In Section 2 we present the results of analysis of the microquasar GRS 1915+106 observations, obtained by the *Rossi X-ray Timing Explorer* (RXTE). The X-ray lightcurves were examined to determine the time lags between hard and soft X-ray bands in different modes characteristic for the variability of this source. In Section 3 we describe our model and assumptions about the disc and corona structure. The initial state of the disc plus corona system, as well as the prescription for the mass exchange, are described in Section 3.1, while the time-dependent equations, according to which this system subsequently evolves with time, are given in Section 3.2. The results of the evolution are given in Section 4. We discuss our model and compare its predictions with observations in Section 5. The conclusions are given in Section 6.

* E-mail: agnes@camk.edu.pl

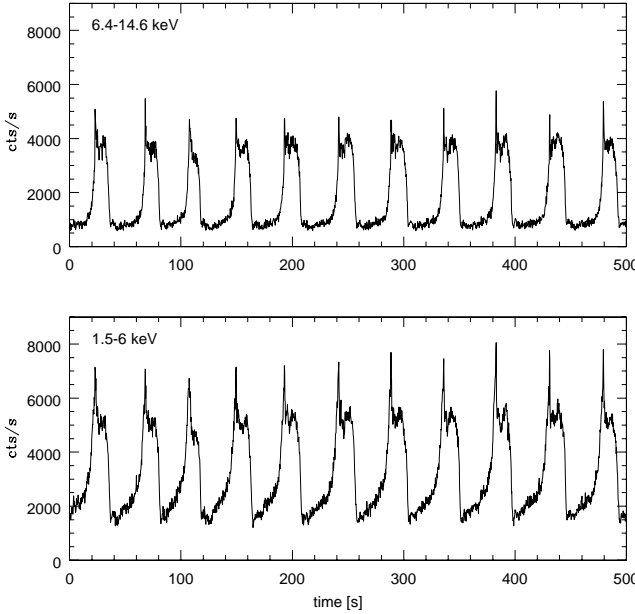


Figure 1. The X-ray lightcurves of GRS 1915+105 obtained from RXTE observation from June 20 2000 (class ρ), in the energy bands 1.5-6 keV and 6.4 - 14.6 keV.

2 TIME DELAYS

Fourier resolved time delays in the lightcurves of GRS 1915+105 were analysed by Muno et al. (2001) for the periods of extended hard steady state. In the present paper we concentrate mostly on periods with significant outbursts. In this case Fourier resolved phase lag approach is not best suited since clear semi-periodic signal dominates each lightcurve. Therefore, we restore to the simplest direct delays, as measured by the cross-correlation function.

In order to determine the time lag between soft and hard X-ray emission we performed the Fourier analysis of these lightcurves by means of the Fast Fourier Transform (FFT) method. The cross-correlation function of two periodic functions $F(t)$ and $G(t)$ is defined as:

$$Corr(\Delta t) = \int F(t)G(t + \Delta t)dt. \quad (1)$$

For our analysis we select lightcurves representative for various variability classes, as studied in detail in Belloni et al. (2000). We choose the exemplary observations of GRS 1915+105 made between 1996 and 2000, available through the public RXTE archive. The data were binned to 0.256 seconds and the lightcurves were generated for the two energy bands separately: 1.5-6 keV (PHA channels 0-14) and 6.4-14.6 keV (PHA channels 15-35). Each lightcurve consists of one or more intervals, and in the subsequent analysis we compare the single intervals between each other.

In Figure 1 we show an exemplary lightcurve of the microquasar observed by RXTE on 20 June, 2000. This variability pattern belongs to the class ρ of Belloni et al. (2000). The cross-correlation function is calculated for the two lightcurves obtained in this observation and shown in Figure 2. The maximum of this cross-correlation function defines the time lag, Δt , between the two lightcurves. In this

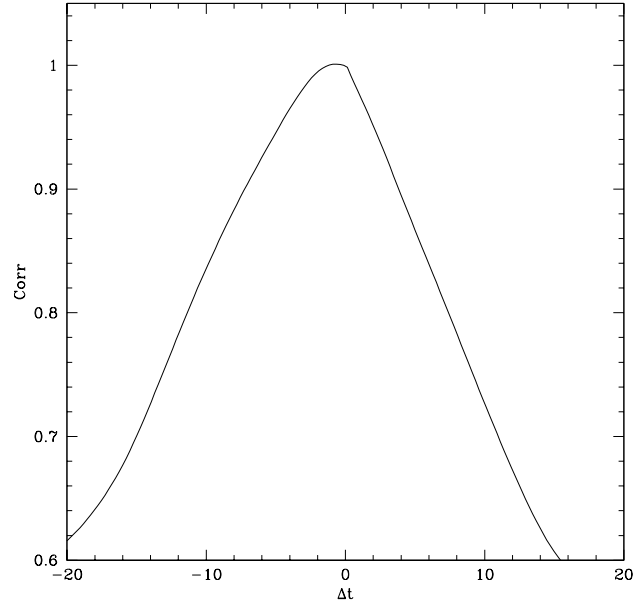


Figure 2. The normalized cross-correlation function of the two lightcurves, 1.5-6 keV and 6.4 - 14.6 keV, shown in Fig. 1. The main peak is shifted to -0.768 s, which means that the hard X-ray lightcurve lags the soft X-ray one by 0.768 s.

Table 1. Time lag of the hard X-ray lightcurve (6.6-14.6 keV) with respect to the soft X-ray lightcurve (1.5-6 keV). Δt_1 is calculated for the non-smoothed lightcurves, binned by 0.256 sec., and Δt_2 is calculated for the lightcurves smoothed over $\Delta T = 1$ s.

PID	Date obs.	Class	Δt_1 [s]	Δt_2 [s]
20402-01-28-00	18/05/97	α	0.0	0.0
20402-01-41-00	19/08/97	δ	0.0	0.0
20402-01-37-00	17/07/97	γ	0.0	0.0
20402-01-44-00	31/08/97	β	0.0	0.0
10408-01-15-00	16/06/96	θ	0.0	0.0
20402-01-36-00	10/07/97	λ	0.0	0.256
20402-01-33-00	18/06/97	κ	0.256	0.512
50703-01-15-01	20/06/00	ρ	0.768	1.024

case it is equal to $\Delta t = 0.768$ s. This means that the hard X-ray lightcurve lags the soft X-ray one by 0.768 seconds, which in this case is roughly 1.5% of the outburst duration. Other results are given in Table 1.

Regular, large timescale outbursts are characteristic for the lightcurves of type ρ and κ . In other cases, the rapid, stochastic variability is overimposed on the more regular outburst pattern of a longer timescale (classes λ , β , and θ) or even dominates the whole observation interval (classes α , δ and γ). This rapid variability does not exhibit any time lags between hard and soft X-ray bands and is probably not correlated with the disc/corona system instability. Therefore, in order to determine more accurately the correlation between hard and soft X-rays in case of long outbursts, we filter out the rapid, small scale variations. We smoothen the lightcurves by applying the running mean filter (Stull 1988), to remove the variations shorter than (arbitrary) $\Delta T = 1$

sec. The resulting time lags are given in the last column of Table 1. We see that the time lags between regular outbursts are even more pronounced, if these outbursts are cleared from the stochastic variability. On the other hand, the time lag Δt_2 remains only marginally detectable, or equal to zero, in the lightcurves that exhibit mostly the stochastic variations.

The measured lags calculated for the two latter observations, κ and ρ , seem to be exceptionally high for an X-ray binary (Życki, private communication). However, this is not surprising since only GRS 1915+105 exhibits outbursts while other sources show only stochastic type of variability, which must be of different nature.

3 TIME-DEPENDENT DISC/CORONA MODEL

Accretion discs are known to be locally unstable in certain temperature (corresponding to the accretion rate) and density ranges, in which the cooling and heating balance is strongly influenced either by atomic opacities or by the radiation pressure. Such instabilities do not disrupt the disc completely, but lead to repetitive outbursts.

The first type of instability, connected with the partial hydrogen ionization (Smak 1984; Meyer & Meyer-Hofmeister 1984), operates in accretion discs of binary systems in the range of radii of the order of $10^4 - 10^5 R_{\text{Schw}}$ and is responsible for the luminosity changes on timescales of months, e.g. Dwarf Nova outbursts.

The other instability, caused by the radiation pressure domination over the gas pressure, operates in the innermost regions of the disc, where the temperature exceeds $\sim 10^6$ K, and is responsible for the disc variability on the shortest timescales (of the order of tens - hundreds of seconds). This radiation pressure instability was first noticed in Pringle, Rees & Pacholczyk (1974) and studied in Lightman & Eardley (1974) and Shakura & Sunyaev (1976). Abramowicz et al. (1988) found that radial advection has stabilizing effect on the disc at high accretion rates and the time-dependent calculations of the disc limit-cycle behaviour were performed by Honma et al. (1991) and by Szuszkiewicz & Miller (1998).

The innermost disc regions in which the radiation pressure instability is possible, are covered by the hot corona. Direct comparison of the extension of the radiation pressure domination zone and the corona covered zone, resulting from the model of the stationary, two-temperature corona, was performed by Janiuk & Czerny (2000). In the time-dependent model of radiation-pressure instability proposed in Janiuk, Czerny & Siemiginowska (2002) we used a simplified description of a stationary corona above the fluctuating disc, parameterized by a constant value of the fraction of gravitational energy dissipated in the corona (f_{cor}). Here we extend our model to the case of a non-stationary corona, that forms due to the continuous evaporation of material from the disc surface. Due to the mass exchange with the disc the corona follows its time-dependent behaviour and therefore periodic changes are expected also in the hard X-ray luminosity.

3.1 Assumptions and model parameters

3.1.1 Disc

First we describe the initial steady state disc model, from which we start our subsequent calculations. Throughout the calculations we use the vertically integrated equations of the disc structure, as the disc geometrical thickness H is always small ($H/r \sim 0.01$ in the quiescent disc and $H/r \sim 0.1$ in the outburst; see Section 4.1).

The angular velocity of the disc is assumed to be Keplerian, $\Omega = \sqrt{GM/r^3}$, and the sound speed is $c_s = \sqrt{P/\rho} = \Omega H$. Here ρ is the gas density in g/cm³, M is the mass of the accreting black hole and G is the gravitational constant. A non-rotating, Schwarzschild black hole is assumed and the inner radius of the disc is always at $3 R_{\text{Schw}}$. The outer radius is equal to $300 R_{\text{Schw}}$, and at this radius a constant mass inflow, parameterized by the external accretion rate \dot{M}_{ext} is assumed. Only the innermost zone up to $\sim 100 R_{\text{Schw}}$ is the subject to radiation pressure instability, while the rest of the disc is stable (the exact value of the radial extension of the unstable zone depends on the model; see Section 4.1). The mass of the black hole is assumed to be $10M_{\odot}$.

For the disc heating we assume that the viscous stress tensor is proportional to the total pressure P :

$$\tau_{r\varphi} = -\alpha P, \quad (2)$$

and the vertically integrated heating rate is

$$Q_{\text{visc}}^+ = \frac{3}{2}\alpha\Omega HP \quad (3)$$

where α is the viscosity parameter given by Equation 7. The total pressure P consists of the gas and radiation pressure:

$$P = P_{\text{rad}} + P_{\text{gas}} \quad (4)$$

$$P_{\text{gas}} = \frac{k}{m_p} \rho T \quad (5)$$

$$P_{\text{rad}} = \frac{1}{3}aT^4 \quad (6)$$

where T is the mid-plane temperature, and k , m_p and a are physical constants.

The angular momentum transport in the accretion disc is driven mostly by the magneto-rotational turbulences (see Janiuk et al. 2004 and references therein). Since the magnetic fields are quickly expelled from the radiation-dominated disc (Sakimoto & Coroniti 1989), the transport efficiency, and in turn the viscosity parameter, must decrease when the radiation pressure becomes dominant. On the other hand, when the contribution from radiation pressure is only moderate, it may still be possible to couple the radiation to the particles. Here we adopt a modified viscosity law for the accretion disc (Chen & Taam 1993; Nayakshin, Rappaport & Melia 2000):

$$\alpha = \alpha_0 \frac{(1 + \xi/\xi_0)}{(1 + (\xi/\xi_0)^2)} \quad (7)$$

where $\xi = P_{\text{rad}}/P_{\text{gas}}$ (for the discussion of this parameterization see Section 5.1). For the model parameters α_0 and ξ_0 we assumed the values 0.01 and 8.0, respectively. This prescription implies that for small to moderate values of ξ we have effectively the disc heating proportional to the total pressure, while for large values of ξ the viscosity is proportional to the gas pressure. Therefore the radiation pressure

instability may still operate, contrary to the so-called β -disc prescription (Lightman & Eardley 1974).

The cooling in the disc is due to advection and radiation and the radiative cooling is equal to:

$$Q_{\text{rad}}^- = \frac{P_{\text{rad}} c}{\tau} = \frac{\sigma T^4}{\kappa \Sigma} \quad (8)$$

where τ is the optical depth, $\Sigma = \rho H$ is the gas column density in g cm^{-2} , c and σ are physical constants, and we adopt the electron scattering opacity $\kappa = 0.34 \text{ cm}^2/\text{g}$.

The advective cooling in a stationary disc is determined from the global ratio of the total advected flux to the total viscously generated flux (e.g. Paczyński & Bisnovatyi-Kogan 1981; Muchotrzeb & Paczyński 1982; Abramowicz et al. 1988)

$$Q_{\text{adv}}^- = \frac{F_{\text{adv}}}{F_{\text{tot}}} = -\frac{2rPq_{\text{adv}}}{3\rho GM} \quad (9)$$

and

$$q_{\text{adv}} = (12 - 10.5\beta) \frac{\partial \ln T}{\partial \ln r} - (4 - 3\beta) \frac{\partial \ln \rho}{\partial \ln r} \quad (10)$$

Here β is the ratio of the gas pressure to the total pressure $\beta = P_{\text{gas}}/P = 1/(1 + \xi)$. In the initial stationary disc we assume that q_{adv} is approximately constant and of the order of unity (in the subsequent evolution the advection will be calculated more carefully, with appropriate radial derivatives).

In order to calculate the initial steady-state configuration, we solve the energy balance: $F_{\text{tot}} = Q_{\text{visc}}^+ = Q_{\text{adv}}^- + Q_{\text{rad}}^-$. Here the total energy flux F_{tot} dissipated within the disc at a radius r is calculated as:

$$F_{\text{tot}} = \frac{3GM\dot{M}}{8\pi r^3} f(r) \quad (11)$$

where

$$f(r) = \left(1 - \left(\frac{3R_{\text{Schw}}}{r}\right)^{3/2}\right) \frac{r - R_{\text{Schw}}}{2R_{\text{Schw}}} \quad (12)$$

is the boundary condition in the pseudo-Newtonian potential (Paczyński & Wiita 1980). We choose the initial accretion rate \dot{M} that is constant throughout the disc and is low enough for the disc to be on the stable gas-pressure dominated branch, where neither radiation pressure nor advection is important (see Figure 3). The initial model is calculated by means of a simple Newtonian method, through which we determine the radial profiles of density and temperature, as well as the disc thickness.

3.1.2 Corona

The corona is assumed to be geometrically thick and optically thin. Therefore its height is assumed to be equal to radius, $H_{\text{cor}} = r$, and the pressure in the corona is only gas pressure due to ions:

$$P_{\text{cor}} = P_{\text{gas}} = \frac{k}{m_p} \rho_{\text{cor}} T_{\text{cor}} \quad (13)$$

The contribution from the electrons is neglected. The corona is hot and its ion temperature is assumed to be equal to the virial temperature:

$$T_{\text{cor}} = T_{\text{vir}} = \frac{GM}{r} \frac{m_p}{k} \quad (14)$$

The initial configuration of the corona is computed under the assumption that its optical depth is equal to unity:

$$\tau_{\text{cor}} = \kappa \Sigma_{\text{cor}} = 1.0 \quad (15)$$

and therefore the corona has a uniform surface density. When the time evolution starts, the proper solution develops in the middle parts of the disc, but will be fixed at the boundaries R_{in} and R_{out} by the above condition.

3.1.3 Mass exchange (prescription I)

The mass exchange rate in the vertical direction, between the disc and corona, is equal to the ratio between the locally generated flux used to evaporate the disc material and the energy change per particle:

$$\dot{m}_z = \frac{F}{\Delta E/m_p} = \frac{F m_p}{k T_{\text{cor}}} \quad (16)$$

(measured per surface unit, g/s/cm^2).

In a stationary disc the generated flux depends on the accretion rate and the disc radius (see Eq. 11). We assume that during the time evolution the energy flux leading to evaporation preserves this dependence. Since both the energy dissipated within the corona and within the disc can lead to disc evaporation, we assume that the energy flux is proportional to the sum of the disc and corona accretion rates, taken with different numerical coefficients: $F \propto (0.5B_1 \dot{M}_{\text{cor}} + B_2 \dot{M}_{\text{disc}})$. The coefficients B_1 and B_2 are in the range from 0 to 1 and express the fraction of the generated flux that is used to drive the evaporation. The share of the corona is always lower than the half of the total corona flux, since half of the flux from the corona is directed toward the observer, whereas the other half is directed towards the disc and there reprocessed.

The total accretion rate is $\dot{M} = \dot{M}_{\text{cor}} + \dot{M}_{\text{disc}}$ and may be locally constant in case of a stable disc. When the disc is unstable, both local accretion rates strongly depend on time and radius, and the relative contribution of the disc and corona to the total flow also vary.

Expressing the accretion rates through the local variables $\dot{M}_{\text{cor}} = 2\pi \Sigma_{\text{cor}} r v_r^{\text{cor}}$ and $\dot{M}_{\text{disc}} = 2\pi \Sigma_{\text{disc}} r v_r^{\text{disc}}$ in the corona and disc respectively, we obtain a useful formula for the vertical mass transfer:

$$\dot{m}_z = \frac{3}{4r} f(r) (0.5B_1 \Sigma_{\text{cor}} v_r^{\text{cor}} + B_2 \Sigma_{\text{disc}} v_r^{\text{disc}}) \quad (17)$$

This formula is qualitatively similar to $\dot{m}_z \sim \dot{M}_{\text{cor}}^{5/3}/r^{3/2}$, derived by Różańska & Czerny (2000) under specific assumptions about the disc/corona coupling. However, their model described a stationary evaporation and did not depend on time. In our case the corona has to develop above the disc from the initial, uniform, very low density distribution, and this rise is provided by the sum of disc and corona accretion rates. (In the above, we denoted the quantities in the disc with the subscript “disc”, in order to discriminate them from the coronal ones. Please note, that whenever the physical quantities appear without any subscript, they also refer to the disc, and the coronal quantities are always distinguished with the subscript “cor”.)

3.2 Time evolution

Having computed the initial disc and corona state we allow the density and temperature of the disc and the density of the corona to evolve with time. We solve the equation of mass and angular momentum conservation:

$$\frac{\partial \Sigma}{\partial t} = \frac{1}{r} \frac{\partial}{\partial r} (3r^{1/2} \frac{\partial}{\partial r} (r^{1/2} \nu \Sigma)) - \dot{m}_z \quad (18)$$

and the energy equation:

$$\begin{aligned} \frac{\partial T}{\partial t} + v_r \frac{\partial T}{\partial r} = & \frac{T}{\Sigma} \frac{4 - 3\beta}{12 - 10.5\beta} \left(\frac{\partial \Sigma}{\partial t} + v_r \frac{\partial \Sigma}{\partial r} \right) \\ & + \frac{T}{PH} \frac{1}{12 - 10.5\beta} (Q^+ - Q^-). \end{aligned} \quad (19)$$

Here

$$v_r = \frac{3}{\Sigma r^{1/2}} \frac{\partial}{\partial r} (\nu \Sigma r^{1/2}) \quad (20)$$

is the radial velocity in the disc while $\nu = (2P\alpha)/(3\rho\Omega)$ is the kinematic viscosity. The heating term is given by Equation 3 and the cooling term Q^- is given by Equation 8, while the advection is included in the energy equation via the radial derivatives.

The evolution of the coronal density is given by mass and angular momentum conservation in the corona:

$$\frac{\partial \Sigma_{\text{cor}}}{\partial t} = \frac{1}{r} \frac{\partial}{\partial r} (3r^{1/2} \frac{\partial}{\partial r} (r^{1/2} \nu_{\text{cor}} \Sigma_{\text{cor}})) + \dot{m}_z. \quad (21)$$

The radial velocity in the corona is calculated as:

$$v_r^{\text{cor}} = \frac{3}{\Sigma_{\text{cor}} r^{1/2}} \frac{\partial}{\partial r} (\nu_{\text{cor}} \Sigma_{\text{cor}} r^{1/2}) \quad (22)$$

with $\nu_{\text{cor}} = (2P_{\text{cor}}\alpha_{\text{cor}})/(3\rho_{\text{cor}}\Omega)$ and constant viscosity parameter in the corona $\alpha_{\text{cor}} = 0.01$. There is no need to consider the thermal evolution of the corona, since its temperature is always equal to the virial temperature and does not vary with time.

We solve the above set of three time-dependent equations using the convenient change of variables, $y = 2r^{1/2}$ and $\Xi = y\Sigma$, at the fixed radial grid, equally spaced in y (see Janiuk et al. 2002 and references therein). The number of radial zones is set to 216. After determining the solutions for the first 600 time steps by the fourth-order Runge-Kutta method, we use the Adams-Moulton predictor-corrector method, allowing the time-step to vary, when needed.

We choose the no-torque inner boundary condition, $\Sigma_{\text{in}} = T_{\text{in}} = 0$ for the disc. The outer boundary of the disc is parameterized by an external accretion rate \dot{M}_{ext} . If this accretion rate is high enough, the inner disc parts gradually heat themselves and finally end in the unstable regime, forcing the disc to oscillate. The boundary conditions in the corona are given by Equation 15.

4 RESULTS

4.1 Surface density and temperature evolution

The local solutions of the accretion disc model, in the surface density vs. temperature ($\Sigma - T$) plane, can be calculated for a stationary disc in the range of accretion rates. (Alternatively, on the vertical axis we can have accretion rate \dot{M} instead of the disc temperature.) These solutions lie along

the S-shaped stability curve, whose position on the diagram depends on the model parameters: black hole mass, viscosity and radius (c.f. Janiuk et al. 2002, Figs. 1, 3).

Both upper and lower branches of the S-curve are viscously and thermally stable. On the lower stable branch the gas pressure dominates; the middle branch is unstable (radiatively cooled and radiation pressure dominant), as shown in detail by Pringle, Rees & Pacholczyk (1974) and Lightman & Eardley (1974). The upper branch is stabilized in our model again by the dominant gas pressure, due to the modified viscosity law. In case of the standard viscosity (with constant α) this branch would be stabilized mainly by advection, as shown in Abramowicz et al. (1988). In our case the advection is also taken into account, but its role is never dominant.

The S-curve can also be plotted in the $\dot{M} - \Sigma$ plane, for any chosen disc radius. This means that the temporary local solutions are determined by the mean (i.e. external) accretion rate in the disc. Whenever the external accretion rate is low, so that at all the radii in the disc the local solution sits on the lower, stable branch, the accretion proceeds with this rate, which is constant throughout the disc and constant in time. But if the accretion rate is higher than some critical value, $\dot{M}_{\text{ext}} > \dot{M}_{\text{crit}}$, the solutions in the innermost annuli will find themselves on the unstable branch. The higher \dot{M}_{ext} , the more disc annuli will be unstable. This leads to the disc fluctuations, since the accretion cannot proceed smoothly in the unstable mode. Therefore the local accretion rate in the innermost strips changes periodically between the lower and upper stable solutions, being no longer equal to \dot{M}_{ext} (the accretion rate starts to depend on radius and time). This is displayed in the local diagrams $\Sigma - T$ that are resulting from the *time-dependent* model.

The exemplary stability curves of the accretion disc, calculated at several radii from the stationary disc model, are shown in Figure 3 (thin solid lines). The thick points represent the subsequent solutions of the time-dependent model.

The evolution of the disc on the surface density - temperature plane proceeds at first along the lower stable branch, up to the instability region. This is forced by the value of the external accretion rate parameter, which has to be large enough to drive the disc to the unstable configuration. Here we assumed $\dot{M}_{\text{ext}} = 1.5 \times 10^{19} \text{ g s}^{-1}$, which is equal to 0.45 of the Eddington rate (for black hole mass of $10 M_{\odot}$ and efficiency of 1/16). The critical accretion rate in our model depends on whether the corona covers the disc or not; $\dot{m}_{\text{crit}} = 0.05$ for the plain disc, while in the case of a disc/corona system the corona has a stabilizing role and the critical accretion rate is about $\dot{m}_{\text{crit}} = 0.2$. The accretion rates within the range $7.5 \times 10^{18} - 2.6 \times 10^{19} \text{ g s}^{-1}$, were obtained for soft states of GRS 1915+105 by Sobolewska & Życki (2003).

Firstly, in the starting, steady configuration we assumed the accretion rate of $\dot{m} \sim 1.5 \times 10^{-2}$ of the Eddington rate throughout the disc. Therefore at the beginning of the subsequent time-dependent calculations the model has to saturate at the temperatures and densities imposed by the value of \dot{M}_{ext} , imposed at the outer disc radius.

Next, the evolution proceeds in a form of loops between the lower and upper branches. Each loop refers to a single cycle of the instability, and the size of this loop depends on

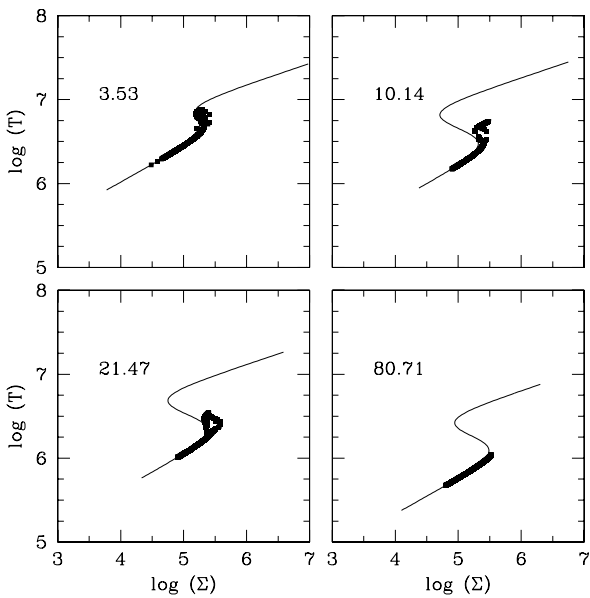


Figure 3. Local evolution of the disc on the surface density - temperature plane, plotted for 4 values of radius: 3.53, 10.14, 21.47 and 80.71 R_{Schw} . The thin solid line marks the stability curve resulting from the initial steady disc model, and the solid points are time-dependent solutions.

the location in the disc. For larger radii the loops become smaller and finally, in the outer disc regions (above $\sim 80 - 100 R_{\text{Schw}}$), there are no instabilities and the disc remains stable all the time. The exact value of the maximal radius of the instability zone depends again on the model. In case of a plain disc, for the external accretion rate $\dot{m}_{\text{ext}} = 0.45$ it is $R_{\text{max}} = 100 R_{\text{Schw}}$, while for $\dot{m}_{\text{ext}} = 0.56$ it is $R_{\text{max}} = 110 R_{\text{Schw}}$. In case of the disc with corona the extension of the unstable zone is respectively $R_{\text{max}} = 80 R_{\text{Schw}}$ and $R_{\text{max}} = 90 R_{\text{Schw}}$.

Note, that in the initial steady disc model we use a simplified parameterization of advection, with $q_{\text{adv}} = 1.0$ (see Equation 10). Therefore the upper stable branch does not represent exactly the advective branch that results from the time-dependent calculations, which are based on the equations with radial derivatives. In fact, q_{adv} is not constant throughout the disc and should depend on radius. However, this initial simplification does not influence our results, since our starting model is located on the lower, gas pressure dominated branch. Here the advection is negligible, and the subsequent time-dependent solutions match the stability curve perfectly.

In Figure 4 we show the radial profiles of the surface density in the accretion disc, in several snapshots during such a loop (one instability cycle). In the minimum of a cycle the surface density in the inner parts of the accretion disc has a flat radial distribution. When the outburst starts, there appears a sharp density peak in the outer part of the unstable zone, which then moves outward. In the maximum of the cycle this peak is accompanied by the largest fluctuation in the density distribution. The reason for these fluctuations are the viscosity and angular momentum trans-

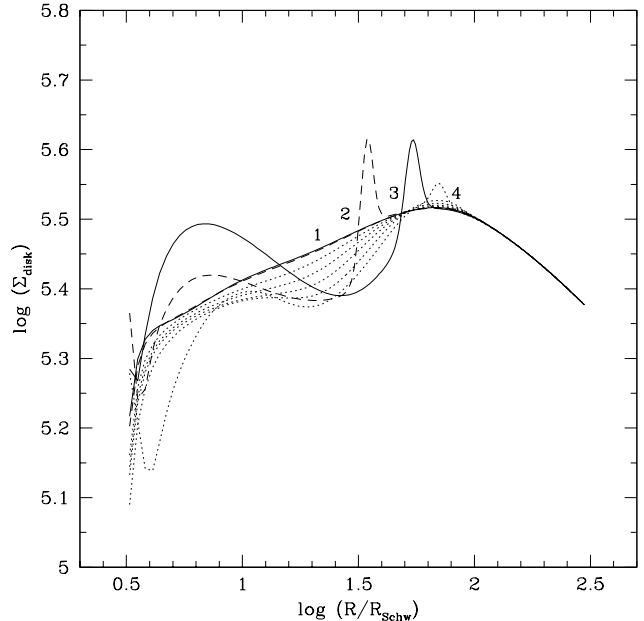


Figure 4. Radial profiles of the disc surface density during the cycle of the evolution. The snapshots were made every 80 seconds and the whole cycle lasts for 625 seconds. The solid curve (1) refers to the minimum of the cycle (lowest disc luminosity, see also Figs. 6 and 8), the dashed curve (2) refers to the rise phase and the solid curve (3) refers to the maximum of the cycle. The dotted line (4) and other dotted lines (unnumbered) refer to the decay phase.

fer changes inside this propagating “density wave”. When the innermost radii of the disc switch to the hot state, the geometrical thickness of this region also rises, thus giving the rise to the kinematic viscosity. The increased transport rate results in the temporary density decay in the unstable zone, as the material starts to fall faster into the black hole. Simultaneously, at the inner edge of the disc there forms a temporary “bump” of material, forced by the no-torque inner boundary condition.

The density fluctuation subsequently vanishes in the end of the cycle and during the decay phase the surface density in the unstable zone gradually rises, to reach the starting configuration.

The corona evolves on a timescale much shorter than the disc. First, we investigate the corona formation in case of no mass exchange with the disc ($B_1 = B_2 = 0$). The initial distribution of the surface density in the corona was flat, as determined by Equation 15. When the evolution starts, the corona very quickly achieves its final shape – the surface density distribution saturates after ~ 125 sec. At the same time the disc evolves very slowly, being ready to start its oscillations after $\sim 10^4$ sec. of a gradual rise in density and temperature. Since there is no coupling with the corona, these oscillations do not influence the corona structure.

Secondly, we proceed with the evolution in case of a substantial mass exchange between the disc and corona ($B_1 = B_2 = 0.5$). In this case, the evaporation of the disc accelerates the corona formation, and after ≤ 100 seconds the coronal surface density in the maximum of the radial

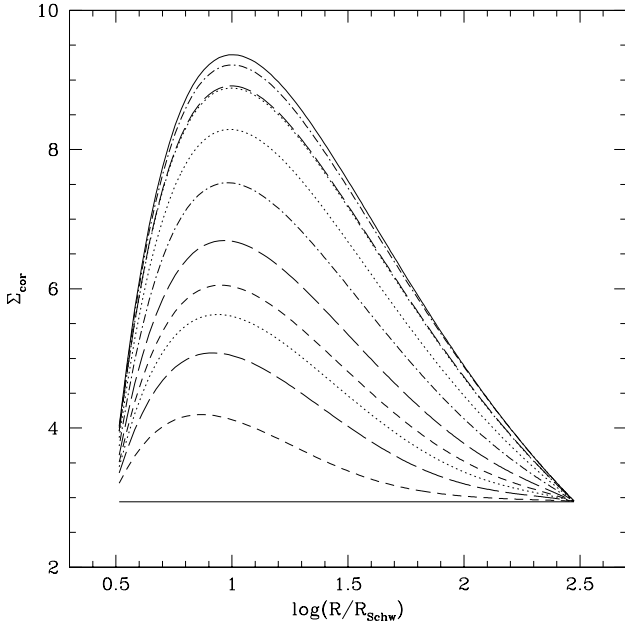


Figure 5. Radial profiles of the corona surface density in case of no mass exchange with the disc ($B_1 = B_2 = 0$). The profiles were calculated every 10 seconds and the density saturated at its final profile after ~ 125 seconds of the evolution.

distribution (around $10R_{\text{Schw}}$) exceeds 10 g/cm^2 . Then the corona is further fed with material by the disc as its evolution proceeds along the stability curve and the coronal surface density further gradually increases. The maximum surface density saturates at $\sim 80 \text{ g/cm}^2$ after the disc reaches the critical point on the stability curve, which determines the maximum density in the disc.

When the disc oscillations start, the corona also follows its time-dependent behavior. In Figure 6 we plot the surface density distribution in the corona during one cycle of the disc instability. The curves are plotted every 80 seconds in case of a full cycle lasting ~ 625 seconds. The solid line (1) is the coronal density in the minimum of the disc limit cycle, the dashed line (2) corresponds to the rise phase of the disc outburst and the solid line (3) corresponds to the maximum of the cycle (outburst). Immediately after the outburst the coronal density distribution comes back to the initial configuration (dotted lines) and remains there for the most of the cycle (4). Therefore during the decay phase of the disc, when the disc surface density gradually changes to reach a flat distribution, there is no change of the density in the corona.

In Figure 7 we show the rate of the mass exchange between the disc and corona, \dot{m}_z , during the disc instability cycle. In the minimum of the cycle the evaporation rate is very low and the maximal mass supply to the corona is achieved at $r \sim 6R_{\text{Schw}}$. When the disc outburst starts, the evaporation rate grows dramatically in the middle of the unstable zone, while dropping to $\dot{m}_z < 0$ at the outer edge of this zone. This is why the corona collapses locally at the outer parts, while expanding slightly in the inner parts during the disc outburst. In the decay phase the evaporation rate again

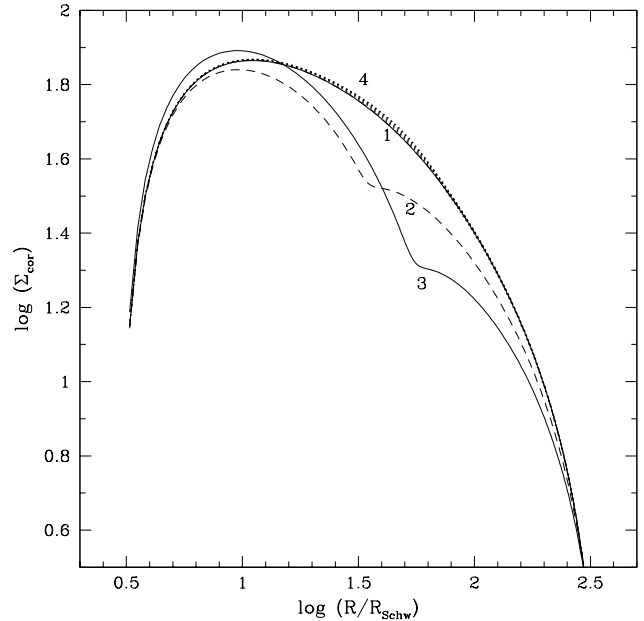


Figure 6. Radial profiles of the corona surface density during the cycle of the evolution. The snapshots were made every 80 seconds and the whole cycle lasts for 625 seconds. The labels are the same as in Fig. 4.

becomes low, with a decaying fluctuation at the outer edge of the instability zone.

4.2 Lightcurves

The lightcurves represent the luminosity of the disc and corona separately. For the optically thick disc the luminosity is given by:

$$L_{\text{disc}} = \int_{R_{\text{min}}}^{R_{\text{max}}} Q_{\text{rad}}^- 2\pi r dr = \frac{4\sigma}{3\kappa} \int_{R_{\text{min}}}^{R_{\text{max}}} \frac{T^4}{\Sigma} 2\pi r dr \quad (23)$$

The luminosity of the corona is calculated under the assumption that the corona is in the thermal equilibrium. The ions are heated by the viscous dissipation and either cool by advection or transfer their energy to the electrons, which in turn radiate e.g. in the Inverse Compton process. Therefore we have:

$$Q_{\text{cor}}^- = Q_{\text{cor}}^+ - Q_{\text{adv}}^- = \frac{3}{2} \Omega \alpha_{\text{cor}} P_{\text{cor}} H_{\text{cor}} - P_{\text{cor}} r v_{\text{r}}^{\text{cor}} \left(\frac{3}{2} \frac{\partial \ln T_{\text{cor}}}{\partial r} - \frac{\partial \ln \Sigma_{\text{cor}}}{\partial r} \right) \quad (24)$$

and

$$L_{\text{cor}} = \int_{R_{\text{min}}}^{R_{\text{max}}} Q_{\text{cor}}^- 2\pi r dr \quad (25)$$

In Figure 8 we show an exemplary lightcurve calculated for several cycles of the disc outburst. The disc limit cycle is very strong since $\dot{M}_{\text{ext}} = 1.5 \times 10^{19} \text{ g s}^{-1}$ substantially exceeds the critical value. Therefore the loops marked by the time-dependent solutions on the $\Sigma - T$ plane encompass substantial range of temperatures and densities, and the unstable region of the disc has the radial extension up to about

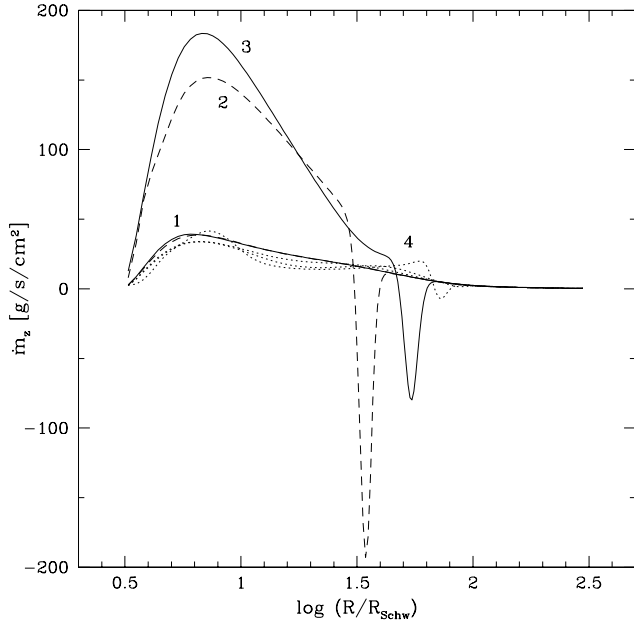


Figure 7. Radial profiles of the mass exchange rate during the cycle of the evolution. The snapshots were made every 80 seconds and the whole cycle lasts for 625 seconds. The labels are the same as in Fig. 4.

$80 R_{\text{Schw}}$. This results in regular, large amplitude outbursts of $\Delta \log L = 0.9$ and $\Delta t = 625$ s. The luminosity variations in the corona, however of the same frequency, are not that strong. Also, they are sometimes anti-correlated with the luminosity changes in the disc, since at the disc rise phase the coronal luminosity at first drops and then rises slightly, to drop and rise again during the disc decay phase. Characteristically, between the disc outbursts the coronal luminosity decreases very slowly, with $\Delta \log L_{\text{cor}}/\Delta t \approx 10^{-5}$, whereas the disc luminosity rises gradually, forming a 'wing' preceding the main outburst.

4.3 Accretion rate

The mass exchange rate in our prescription depends on the accretion rates in the disc and corona (Equation 17). Since they strongly vary with time during the cycle of the disc evolution, the mass exchange can have locally negative value. This has been shown in Figure 7.

In Figures 9 and 10 we show the radial profiles of the accretion rates in the disc and corona, taken in different phases of the cycle: between the disc outbursts (corresponding to phase "1" in Fig. 7) and in the outburst peak (phase "3").

In the minimum of the cycle, i.e. between the outbursts, the accretion rate in the inner parts of the disc, where most of the dissipation takes place, is relatively low. It rises substantially in the maximum of the cycle, therefore causing the disc luminosity outburst. The coronal accretion rate does not change that much, and the corresponding luminosity changes are not very pronounced. This is because in certain radii, at the outer edge of the instability strip, the radial velocity becomes negative. In consequence, the both accretion rates and mass exchange rate, \dot{m}_z , also become negative,

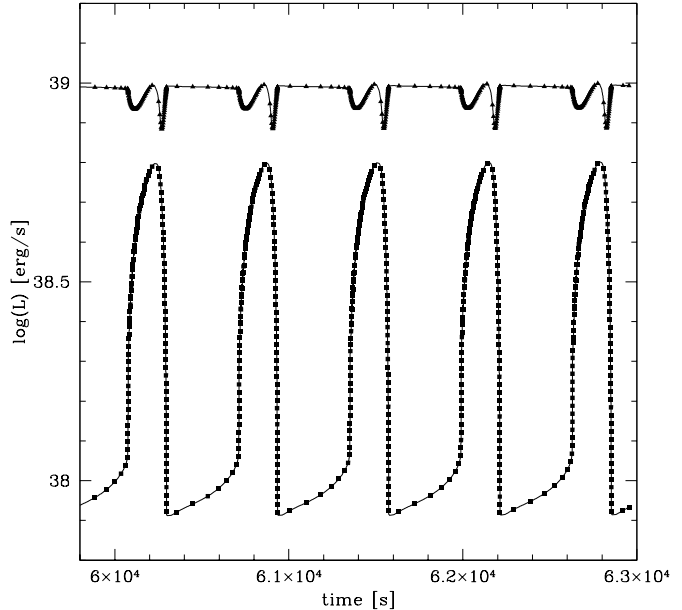


Figure 8. The time evolution of the disc and corona luminosity. Lower curve shows the luminosity outbursts of the disc, while the upper curve shows the simultaneous coronal fluctuations. The external accretion rate is $\dot{M}_{\text{ext}} = 1.5 \times 10^{19}$ g/s.

which means that some amount of material that has been evaporated to the corona, now goes back and sinks in the disc. Negative values of \dot{m}_z are not unphysical: stationary models based on the disc-corona mass exchange of Różańska & Czerny (2000) predict coronal condensation at some radii for high accretion rates. The coronal surface density, and in turn the dissipation rate, is therefore reduced, even in the inner regions, as the mass is spread out over the whole corona. The temporary loss of the accretion rate can be estimated as $\Delta \dot{M} = 4\pi r \dot{m}_z \Delta r$ and it can be as high as 1.9×10^{18} g/s. Therefore almost the whole rise of the coronal accretion rate (and luminosity), triggered by the disc outburst, is immediately compensated by this loss due to the sinking of material in the strip around $\sim 50R_{\text{Schw}}$.

In addition, the accretion rate in the corona is negative in the outermost radii. The extension of this zone of negative \dot{M}_{cor} depends on the outer boundary condition in the corona, which in our case is fixed by $\Sigma_{\text{cor}}(r_{\text{out}}) = 1/\kappa \approx 2.94$. It implies that $\dot{M}_{\text{cor}} < 0$ for $r > 100R_{\text{Schw}}$, so the material slowly flows out from the corona at its outer radius.

4.4 Alternative prescription for the mass exchange (prescription II)

In the above used prescription for the rate of mass exchange between the disc and corona we expressed the total locally generated flux as proportional to the sum of the accretion rates in the disc and corona. In case of a steady-state disc this is equivalent to the sum of the locally generated fluxes by the viscous energy dissipation. However, when we consider the time evolution of an unstable disc, the radial velocity, and in turn the accretion rate, can have locally negative values in some parts of the disc. This forces the mass

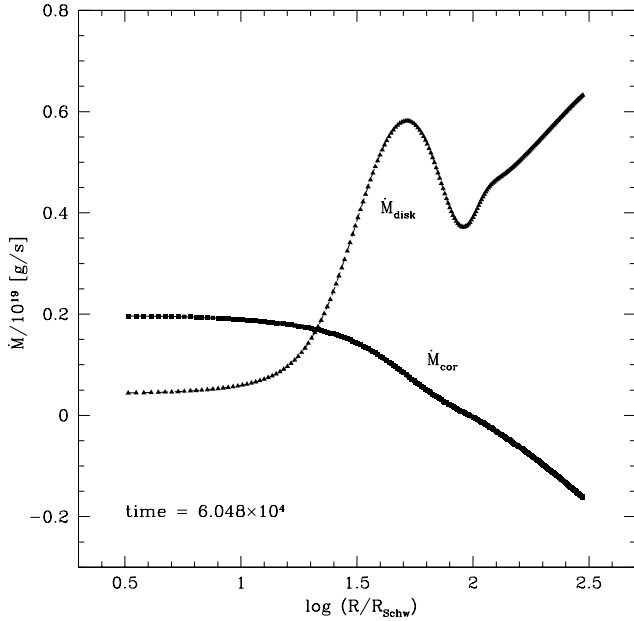


Figure 9. Radial profiles of the accretion rate in the disc (triangles) and in the corona (squares) between the disc outbursts. The time refers to the lightcurve shown in Fig. 8.

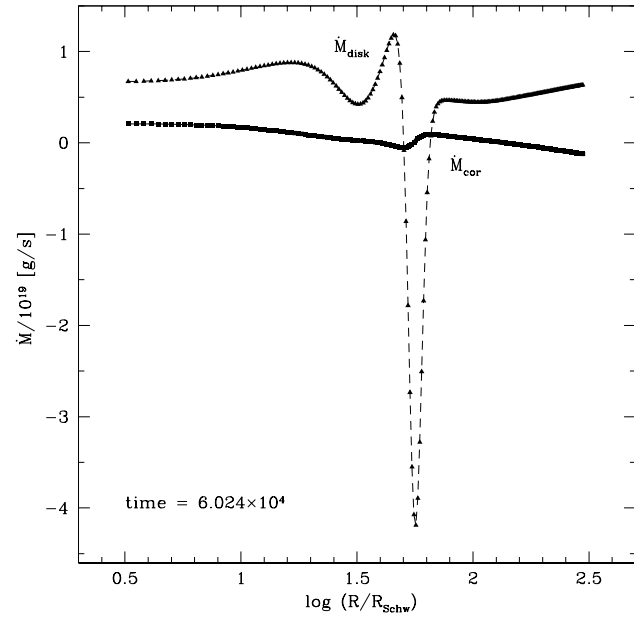


Figure 10. Radial profiles of the the accretion rate in the disc (triangles) and in the corona (squares) in the outburst. The time refers to the lightcurve shown in Fig. 8.

exchange rate to locally decrease in the state of the disc outburst, which is not the case for the viscously generated flux. In other words, the prescription for the mass exchange rate in the outburst of an unstable disc is no longer equivalent to the sum of the locally dissipated fluxes.

Now we check whether the other, more 'conservative'

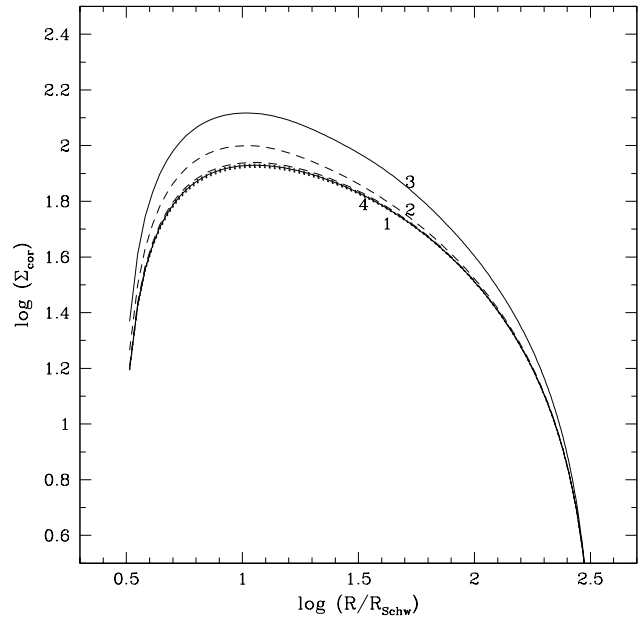


Figure 11. Radial profiles of the corona surface density during the cycle of the evolution for the case of the mass exchange rate given by Eq. 26. The snapshots were made every 80 seconds and the whole cycle lasts for 625 seconds. The labels are the same as in Fig. 4.

prescription for the mass exchange rate can lead to different results of the time evolution of the disc plus corona system. Instead the formula for the vertical mass transfer given by Equation 17, we use the following:

$$\dot{m}_z = \frac{3}{2} \frac{\Omega r}{GM} f(r) \left(0.5 B_1 \alpha_{\text{cor}} \Sigma_{\text{cor}} \frac{GM}{r} + B_2 \alpha_{\text{disc}} P_{\text{disc}} H_{\text{disc}} \right) \quad (26)$$

This form means that the evaporation is proportional to the sum of the energy dissipation rates in the disc and in the corona, and therefore is always positive.

In Figure 11 we show the distribution of the coronal surface density during one cycle of the viscous-thermal instability (cf. Fig. 6). Clearly, there is no local dip in the corona that would be caused by the negative value of \dot{m}_z during the disc outburst, as it was in the previous case. The material does not sink from the corona into the disc anywhere, but is uniformly evaporated and the rate of the evaporation is the highest when the disc is the most luminous.

Similarly, the total luminosity in the corona is now correlated with the disc luminosity. In Figure 12 we show the lightcurves analogous to those in Figure 8. Between the outbursts the coronal luminosity is slightly increasing, and the lightcurve exhibits regular peaks, simultaneous to the disc outbursts. The luminosity changes in the corona are of the order of $\Delta \log L_{\text{cor}} = 0.3$.

4.5 Hard versus soft luminosity: time lags and luminosity-color diagram

Since the mass exchange prescription (II) determined by Equation (26) gave more satisfactory representation of the time evolution with respect to the observed behaviour of

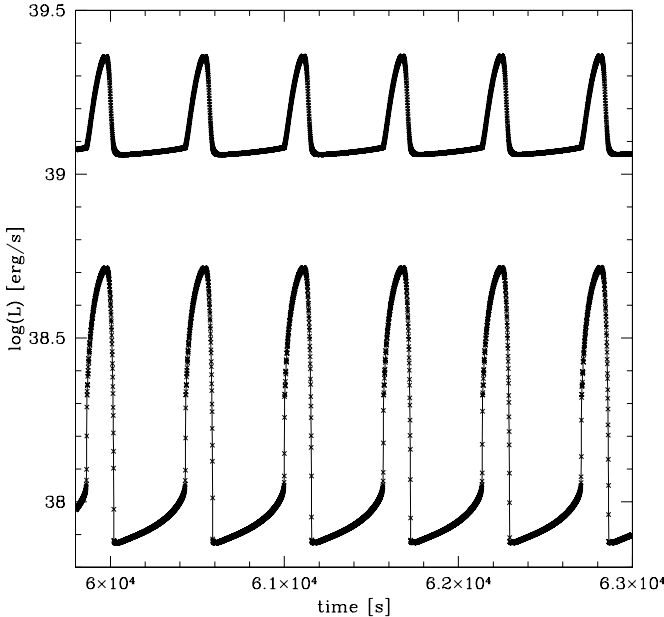


Figure 12. The time evolution of the disc and corona luminosities, for the case of the mass exchange rate given by Eq. 26. Lower curve shows the luminosity outbursts of the disc, while the upper curve shows the simultaneous coronal outbursts. The external accretion rate is $\dot{M}_{\text{ext}} = 1.5 \times 10^{19}$ g/s.

GRS 1915+105, we adopt this prescription in further analysis.

We calculated the cross-correlation function, as defined by Equation (1), for the theoretical lightcurves plotted in Figure 12. Our points were separated at least by 0.039 s, and we found that the corona lightcurve lags the disc by 1.16 seconds. This is shown in Figure 13. The time lag in this case is equal to about 0.5% of the duration of an outburst. We note that the outburst duration depends on the external accretion rate \dot{M}_{ext} and the lag depends on the coronal viscosity parameter α , so we could obtain a range of values for different model parameters.

In Figure 14 we show the luminosity-color diagram for one of the observations of GRS 1915+105, that shows the pronounced outbursts (class ρ , cf. Table 1). On the horizontal axis we plot the soft X-ray flux in the range 1.5–6 keV, and on the vertical axis we plot the X-ray color, i.e. the ratio of the hard to soft fluxes, $F_{6.4-14.6\text{keV}}/F_{1.5-6\text{keV}}$. During its evolution, the source follows a characteristic track, in the form of a loop on this diagram. In the lower region (the “banana” shape) the soft luminosity is low, and the X-ray color is soft. The upper region (“island”) shape is characterized by substantial luminosity both in hard and soft X-ray bands.

In Figure 15 we show the result of our modeling. On the horizontal axis of the theoretical luminosity-color diagram we plot the disc luminosity, while in the vertical axis we plot the ratio of the corona to disc luminosities. The “banana” shape is reproduced in our model quite well. However, we do not obtain the other distinct region on this diagram (the “island”). In our simulations the source moves only along the track shown in Fig. 15, and after reaching the end of the

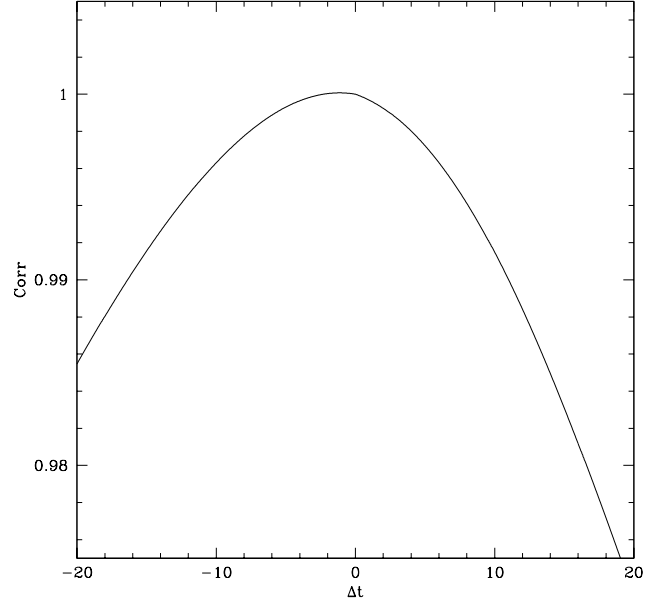


Figure 13. The normalized cross-correlation function of the disc and corona lightcurves. The main peak is shifted to -1.16 s, which means that the corona lightcurve lags the disc one by 1.16 s.

“banana” region immediately jumps to the top-left corner of the diagram.

5 DISCUSSION

The main simplification of our model was the assumption that the temperature in the corona is constant and equal to the virial one. Therefore the corona is heated only via increase of its surface density and is not radiatively coupled to the disc. We do not consider here any specific radiative processes that are important in cooling of the coronal gas, e.g. Comptonization.

On the other hand, this approach lets us solve the set of three time-dependent equations for the disc plus corona evolution, accompanied by the formula for the mass exchange rate, and avoid numerical problems with the fourth equation for the corona temperature. Using a finite time-step we are able to follow the time evolution of the system as long as it saturates in a quasi-stationary state, with oscillations of constant amplitude and duration. We qualitatively and quantitatively check, how the behaviour of the underlying, unstable disc affects the corona and vice versa.

The full, two- or three dimensional treatment to the global long-term evolution of an accretion disc (or disc/corona system) is very complex. Up to now, the sophisticated 2-D and 3-D accretion disc simulations (e.g. Agol et al. 2001; Turner et al. 2003) either treated the problem locally, or did not include radiative cooling. Turner (2004) made the first attempt to compute the 3-D simulation in the flux-limited approximation; in this case however the plasma temperatures are still much too low to form the hot corona. Since the simulations are not able to reach the viscous timescale of the disc, the long-term evolution of an

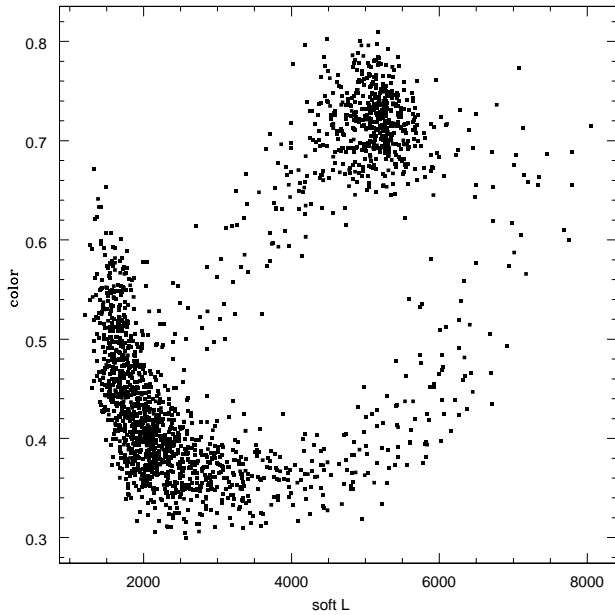


Figure 14. The luminosity-color diagram of the two observed lightcurves, shown in Fig. 1. On the horizontal axis is the soft X-ray flux in the range 1.5-6 keV, and in the vertical axis is the ratio of the hard to soft fluxes, $F_{6.4-14.6 \text{ keV}} / F_{1.5-6 \text{ keV}}$.

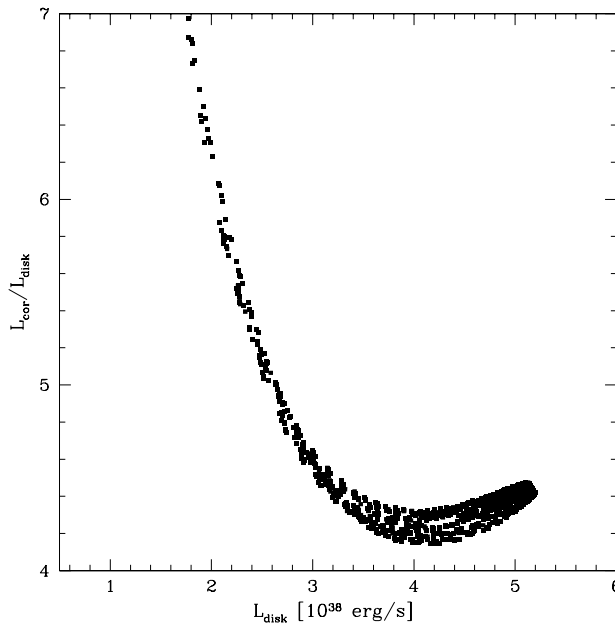


Figure 15. The luminosity-color diagram of the two theoretical lightcurves, shown in Fig. 12. On the horizontal axis is the soft X-ray (disk) luminosity, and in the vertical axis is the ratio of the hard to soft (corona to disk) luminosities.

X-ray source cannot be followed and any observational consequences of such a model are difficult to be checked. Therefore the simple approach presented in this paper can still be valuable.

5.1 Viscosity parameterization

In our choice of the viscosity law we follow the paper of Nayakshin, Rappaport & Melia (2000). The motivation of these authors was mostly observational: they needed a viscosity law which allows for a disc instability at the intermediate accretion rates but provides the stable solution at low and high accretion rates. Moreover, the stable upper branch should appear at accretion rates smaller or comparable to the Eddington rate. The standard αP_{tot} viscosity law of Shakura & Sunyaev (1973) satisfies in a natural way all requirements but the last one. Upper stable branch in such solution forms due to advection (i.e. the “slim disc”; Abramowicz et al. 1988), and the efficient advection develops only for accretion rates much larger than the Eddington values, definitely too high to account for the time behaviour e.g. of the microquasar GRS 1915+105. What is more, in most cases the unstable branch should cease to exist at all since most of the X-ray binaries accreting at high (but sub-Eddington) rates are quite stable and well described by the classical disc (Gierliński & Done 2004).

Therefore, observations tell us that some modifications are absolutely needed. Either we must postulate very strong outflow (which effectively cools the disc), or a modification of the dissipation law itself.

We have much better understanding and numerous observational constraints for the viscosity law when the gas pressure dominates. 3-D MHD simulations of the magnetorotational instability (MRI) well explain the nature of the angular momentum transfer and the rough value of the viscosity parameter. Still, some ad hoc modifications, like additional dependence on the disc thickness, are used to model the development of the ionization instability responsible for outbursts in cataclysmic variables and numerous X-ray transients (e.g. Cannizzo et al. 1995).

The theoretical background of the viscosity law is still quite poor in case when radiation pressure is important. Several authors in the past suggested that actually the whole idea of αP_{tot} scaling is inappropriate, and instead the αP_{gas} should perhaps be used even if the radiation pressure dominates (Lightman & Eardley 1974; Stella & Rosner 1984). Sakimoto & Coroniti (1989) argued that the magnetic field will be expelled from the radiation pressure dominated disc by the buoyancy so the effectiveness of the angular momentum transfer must decrease with an increase of radiation pressure. Other authors argued that whenever radiation pressure dominates, new kinds of instabilities develop which may modify the disc structure considerably. Gammie (1998) discussed the photon bubble instability, and Ruszkowski & Begelman (2003) argued this instability leads to the disc clumpiness which in turn influences the radiative transfer.

We expect some improvement of the viscosity modeling with the future development of MHD simulations of radiation pressure dominated discs. So far, two such simulations were performed. 2-D computations of Agol et al. (2001) lasted only for a fraction of the disc thermal timescale and as a result the disc collapsed to gas pressure dominated state.

A 3-D simulation of the disc which reached the thermal balance and lasted for about 8 thermal timescales was recently completed by Turner (2004). The disc did not achieve the full stability and showed long-lasting variations by a factor of a few but the instability was not as violent as predicted by the standard αP_{tot} mechanism (Suzskejewicz & Miller 1998; Janiuk et al. 2002). The magnetic field lines were indeed partially expelled from the disc interior. In this simulation, the initial Shakura & Sunyaev (1973) state with $\alpha = 0.01$ evolved to a complex state with mean dissipation level equivalent to $\alpha = 0.0013$.

Therefore, the modified viscosity law, given by Eq. 7, seems to be a plausible option in case of the accretion disc. Since in the corona the radiation pressure does not contribute to the total pressure, the classical viscosity parameterization of the corona with constant α is also justified.

5.2 Comparison with observations

Our time dependent model of the non-stationary accretion onto a black hole gives at least a partial explanation of the complex variability of the microquasar GRS 1915+105. Direct evidence for variable accretion rate in this microquasar comes from the spectral analysis (Migliari & Belloni 2003), and a plausible mechanism that leads to the local accretion rate variations in the inner parts of a disc, giving the outbursts of appropriate amplitudes and durations, is the radiation pressure instability.

The microquasar is unique because of its large amplitude, regular outbursts. Such a behaviour is not observed in other Galactic X-ray sources, probably because the Eddington ratio in this microquasar is higher than in other black hole systems (Done, Wardziński & Gierliński 2004). Our model, at least qualitatively, explains this phenomenon. The radiation pressure instability leads to the strong outbursts only if the accretion rate is higher than some critical value. Also, the corona has a stabilizing role and can suppress the disc oscillations completely or make them less pronounced. Quantitatively, however, the reliable determination of the critical accretion rate above which the outbursts occur, would require a more detailed modeling of viscosity within the disc and essentially the 2-dimensional calculations. This is beyond the scope of the present work.

The physical coupling between the disc and corona via the mass exchange leads in a natural way to the regular time delays between the disc (soft X-ray) and corona (hard X-ray) emission. The lag of the order of 1 s is comparable with the viscous timescale in the corona and is required by this hot flow to adjust to the variable conditions in the underlying disc. Such lags are present in some observed lightcurves of the microquasar, i.e. these exhibiting outbursts that are possibly connected with the radiation pressure instability.

The strong variability of GRS 1915+105 manifests itself also by characteristic tracks on the color-color and luminosity-color diagram. The bottom-left corner of the luminosity-color plot is occupied by the source during its gradual rise (the “wing”), preceding the outburst state. This, so called here “banana” shape is well modeled in our calculations. While the disc luminosity (soft X-ray flux) is gradually rising before the outburst, the rise in the coronal luminosity is much flatter, leading therefore to the decreasing hard-to-soft flux ratio (color). On the other hand, in the

outburst peak, when the soft luminosity is the highest, the color starts rising. Just after the outburst there appears a somewhat flat maximum in both hard and soft X-rays, leading to the other distinct region occupied by the source on the luminosity color-diagram: so called here “island” shape. This is not present in our model calculations, since our outburst maximum is a sharp peak. Therefore we do not obtain a state of both high disc and corona fluxes, which in consequence would give the high color in the disc emission peak. Instead, the corona lags the disc emission and its maximum corresponds to the already decaying state of the disc.

6 CONCLUSIONS

We presented the first results of the time-dependent calculations of thermal-viscous evolution of accretion disc that is coupled to the corona by the mass exchange. Contrary to the accretion disc, the corona is stable, since there is only gas pressure included in its equation of state. However, it is also to a certain extent subject to similar changes as the accretion disc during its instability cycle, since it actively responds to the behaviour of the underlying disc.

The main conclusions of the present work are as follows:

- The luminosity outbursts in the disc are correlated with similar outbursts in the corona if the mass exchange rate is proportional to the sum of the locally dissipated fluxes (prescription II). The assumption that it is proportional to the sum of the local accretion rates (prescription I) is equivalent, but only during the disc quiescence. In the outburst this prescription leads to the luminosity dips in the corona rather than outbursts. Specifically, the lightcurves of the disc and corona are anti-correlated, with two dips in the corona corresponding to the peak of the disc luminosity.
- The luminosity profile between the outbursts in the corona is gradually decreasing, while in the disc it is gradually rising (prescription I). Alternatively, the prescription II leads to the slow rise of the coronal flux, correlated with the steep rise of the disc.
- The coronal outbursts are of much smaller amplitude than the disc ones, but of similar duration.
- The outbursts in the corona lag the disc evolution by ~ 1 second, which is in good agreement with observations of the microquasar GRS 1915+105.
- The outer boundary condition in the corona determines if the material flows out at the outer edge. For small surface density $\Sigma_{\text{out}} \sim 3 \text{ g/cm}^2$ the accretion rate in the corona is negative above $\sim 100R_{\text{Schw}}$.
- If the mass exchange between the disc and corona is proportional to the sum of the local accretion rates (prescription I), the material may also locally sink into the disc in the region around $50R_{\text{Schw}}$.

Our model is only in part able to reproduce the tracks of the system on the luminosity-color diagram, having a “banana” shape without the “island” one. This should be modeled in more detail, including also the spectral analysis. In addition, the tracks on the color-color diagram, not analyzed here, in some observed sources may have a form of *hysteresis* (Maccarone & Coppi 2002; Zdziarski et al. 2004). Since the phenomenon is connected with much longer timescales, than those considered here, the underlying instability mechanism

should be different. A plausible one seems to be the partial hydrogen ionization instability, which operates essentially in the same way, causing the disc to oscillate between the cold and hot phases. This is the subject of our future investigations.

ACKNOWLEDGMENTS

We thank Małgorzata Sobolewska for help in data reduction and Agata Różańska, Piotr Życki, Friedrich Meyer and Emmi Meyer-Hofmeister for helpful discussions. This research has made use of data obtained through the HEASARC Online Service, provided by NASA/Goddard Space Flight Centre. This work was supported in part by grant 2P03D00124 of the Polish State Committee for Scientific Research.

REFERENCES

Abramowicz M. A., Czerny B., Lasota J.-P., Szuszkiewicz E., 1988, *ApJ*, 332, 646

Agol E., Krolik J., Turner N.J., Stone J.M., 2001, *ApJ*, 558, 543

Belloni T., Klein-Wolt M., Mendez M., van der Klis M., van Paradijs J., 2000, *A&A*, 355, 271

Cannizzo J.K., Chen W., Livio M., 1995, *ApJ*, 454, 880

Chen X., Taam R.E., 1994, *ApJ*, 412, 254

Done C., 2002, in “X-ray astronomy in the new millennium”, Eds. R. D. Blandford, A. C. Fabian and K. Pounds, Roy. Soc. of London Phil. Tr. A., vol. 360, Issue 1798, p.1967

Done C., Wardziński G., Gierliński M., 2004, *MNRAS*, 349, 393

Gammie C.F., 1998, *MNRAS*, 297, 929

Gierliński M., Done C., 2004, *MNRAS*, 347, 885

Honma F., Matsumoto R., Kato S. 1991, *PASJ*, 43, 147

Janiuk A., Czerny B., 2000, *New Astronomy*, 5, 7

Janiuk A., Czerny B., Siemiginowska A., 2002, *ApJ*, 576, 908

Janiuk A., Czerny B., Siemiginowska A., Szczerba R., 2004, *ApJ*, 602, 595

Meyer F., Meyer-Hofmeister E., 1984, *A&A*, 132, 143

Maccarone T.J., Coppi P.S., 2003, *MNRAS*, 338, 189

Meyer F., Meyer-Hofmeister E., 1994, *A&A*, 288, 175

Mirabel I.F., Rodriguez L.F., 1994, *Nature*, 371, 46

Migliari S., Belloni T., 2003, *A&A*, 404, 283

Muchotrzeb B., Paczyński B., 1982, *Acta Astron.*, 32, 1

Muno M., et al., 2001, *ApJ*, 556, 515

Nailk S., Agrawal P.C., Rao A.R., Paul B., 2002, *MNRAS*, 330, 487

Nayakshin S., Rappaport S., Melia F., 2000, *ApJ*, 535, 798

Lasota J.-P., Pelat D., 1991, *A&A*, 249, 574

Lightman A.P., Eardley D.M., 1974, *ApJ*, 187, L1

Paczyński B. & Bisnovatyi-Kogan G., 1981, *Acta Astron.*, 31, 283

Paczyński B., Wiita P.J., 1980, *A&A*, 88, 23

Pringle J.E., Rees M.J., Pacholczyk, A.G., 1974, *A&A*, 29, 179

Różańska A., Czerny B., 2000, *A&A*, 360, 1170

Ruszkowski M., Begelman M.C., 2003, *ApJ*, 586, 384

Sakimoto P.J., Coroniti F.V., 1989, *ApJ*, 342, 49

Shakura N.I., Sunyaev R.A., 1973, *A&A*, 24, 337

Shakura N.I., Sunyaev R.A., 1976, *MNRAS*, 175, 613

Smak J. 1984, *Acta Astron.* 34, 161

Sobolewska M., Życki P.T., 2003, *A&A*, 400, 553

Stella L., Rosner R., 1984, *ApJ*, 277, 312

Stull R.B., 1988, *An Introduction to Boundary Layer Meteorology*, Kluwer Academic Publishers, Dordrecht

Szuszkiewicz E., Miller J., 1998, *MNRAS*, 298, 888

Taam R. E., Lin D. N. C., 1984, *ApJ*, 287, 761

Taam R. E., Chen X., Swank J.H., 1997, *ApJ*, 485, L83

Turner N.J., Stone J.M., Krolik J.H., Sano T., 2003, *ApJ*, 593, 992

Turner N.J., 2004, *ApJ*, 605, L45

Watarai & Mineshige S., 2003, *ApJ*, 596, 421

Zdziarski A.A., Gierliński M., Mikołajewska J., Wardziński G., Harmon A.B., Kitamoto S., 2004, *MNRAS*, 351, 791